generation of unstable blood vessels that regress over time or functionally immature vessels accompanied with endothelial dysfunction in ischemic areas.[5,9]

The omentum (OM), historically used in surgical revascularization for patients with ischemic heart disease, is also known to release a number of angiogenic cytokines and attenuate inflammation.[10–14] In addition, the gastroepiploic artery involved in the OM-flap can play an important role as an extracardiac blood source with high perfusion capacity for developing effective collateral vessels for advanced coronary artery disease. We established a combination strategy of cell-sheet transplantation covered with a pedicle OM-flap in porcine models, allowing us to implant large numbers of cells and improve cell survival.[13,14] However, data are scarce regarding the therapeutic effects of such combined treatment on vessel maturity and coronary microcirculation physiology in ischemic territory. We hypothesized that cell-sheet transplantation with a pedicle OM-flap will better promote arteriogenesis and stabilize blood vessels in ischemic myocardium along with improved coronary microcirculation physiology, consequently enhancing the therapeutic effects of cell-sheet therapy. Herein, we focused on vessel maturation induced by cell-sheet therapy with an OM-flap and evaluated the physiological benefits in coronary microcirculation utilizing modern modalities such as *in vivo* synchrotron-based microangiography and positron emission tomography (PET).

RESULTS

Histological analysis of host myocardium

Four weeks after treatment, myocardial structural components, collagen accumulation and cardiomyocyte hypertrophy, were assessed by hematoxylin-eosin, Masson trichrome, and Periodic acid-Schiff staining (n = 11 for each group). LV myocardial structure was better maintained in the combined group as compared with the others (**Figure 1c**). The combined group had a significantly thickened anterior LV wall (anterior wall thickness, control 392 ± 31 versus combined 912 ± 34 versus sheet-only 688 ± 27 versus OM-only 500 ± 28 μm) (**Figure 1d**). That group also had a significantly attenuated collagen accumulation (percent fibrosis, 18 ± 1 versus 8 ± 4 versus 13 ± 6 versus 14 ± 1%, respectively) (**Figure 1e**) and cardiac hypertrophy (myocyte size, 23 ± 1 versus 16 ± 1 versus 20 ± 3 versus 21 ± 2 μm, respectively) (**Figure 1f**) in the peri-infarct regions (ANOVA $P < 0.001$ for all).

Gene expressions in peri-infarct myocardium during acute treatment phase

The myocardial gene expressions related to angiogenesis, vessel maturation, and anti-inflammation were analyzed at 3 days after each treatment using real-time PCR (n = 6 for each group). As compared to the others, the combined group showed substantially higher gene expressions of *vascular endothelial growth factor (VEGF)-A*, *VEGF receptor-1*, *VEGF receptor-2*, *Akt-1*, *platelet-derived growth factor (PDGF)-β*, *angiopoietin (Ang)-1*, *Tie-2*, *vascular endothelial (VE)-cadherin*, *platelet endothelial cell adhesion molecule (PECAM)-1*, and *stromal cell-derived factor (SDF)-1* in peri-infarct myocardium at the early stage of transplantation (**Figure 2**).

Vessel recruitment in transplanted cell-sheets and donor cell survial

To evaluate the effect of adding OM-flap to the cell-sheet therapy on the vessel recruitment (angiogenesis) in the transplanted area that should be related to the donor cell survival, we serially assessed the number of functional blood vessels with patent endothelial layers (CD31/lectin double-positive cells) in the transplanted area of the sheet-only and combined groups at 3, 7, and 28 days after each treatment (n = 6 for each group and each time point) (**Figure 3a–f**). At 3 days after treatment, in the sheet-only group, several blood vessels were just located at the border between the sheet and infarct area (**Figure 3a**), whereas a large number of functional vessels was detected proximal to the border between the cell-sheet and OM and within the sheet in the combined group (**Figure 3d**), suggesting that the cell-sheet received blood supply directly from the infarct myocardium and OM. Consequently, the combined group had greater numbers of functional blood vessels in the cell-sheet than the sheet-only group at any follow-up point, although both groups showed steady decrease in the number of vessels during the 28 days (**Figure 3g**).

The quantitative assessments of the donor (GFP-positive) cell presence were also serially performed to elucidate the donor cell dynamics in the sheet-only (**Figure 3a–c**) and combined (**Figure 3d–f**) groups. We traced the transplanted donor cells and found that there was no significant difference in the engrafted area at 3 days after transplantation between the groups, while the subsequent changes in each group were apparently distinctive (**Figure 3h**). During the 7days after the treatment, the amount of decrease in the engrafted area was substantially smaller in the combined group than that in the sheet-only group, resulting in 4.3-fold increased retention of donor cells in the former group. This led to the greater donor cell presence in the combined group persistently (at least until day 28), which was consistent with the amount of vessel recruitment in the cell-sheet.

Vessel remodeling and maturation in peri-infarct myocardium

We serially assessed neovascular vessel maturity in peri-infarct areas at 3 (n = 6 for each group) and 28 days (n = 11 for each group) after treatment (**Figure 4**). Vessel density and structural maturity were quantified as the number of CD31 positive and CD31/α-smooth muscle actin (SMA) double-positive vessels per mm^2, respectively. A maturation index was calculated as the percentage of CD31/α-SMA double-positive vessels to total vessel number. Functionally mature vessels with patent endothelial layers were assessed by lectin injection, which binds uniformly and rapidly to the luminal surface of endothelium, thus labeling patent blood vessels. Vessels positive for CD31 but negative for lectin were regarded as functionally immature and undergoing regression, or that had lost patency.[15,16]

In general, α-SMA signals were located at the outer edges of CD31 staining, indicating pericyte attachment to newly formed endothelium. Three days after treatment, there was no difference in number of CD31-positive cells among the groups, though the combined group showed a trend of greater number of functional blood vessels with patent endothelial layers (CD31/lectin double-positive) and structurally (CD31/α-SMA double-positive) mature vessels, with a higher maturation index (**Figure 4a–g**). Notably, the percentage without lectin staining (CD31$^+$/lectin$^-$) was significantly smaller in the combined group.

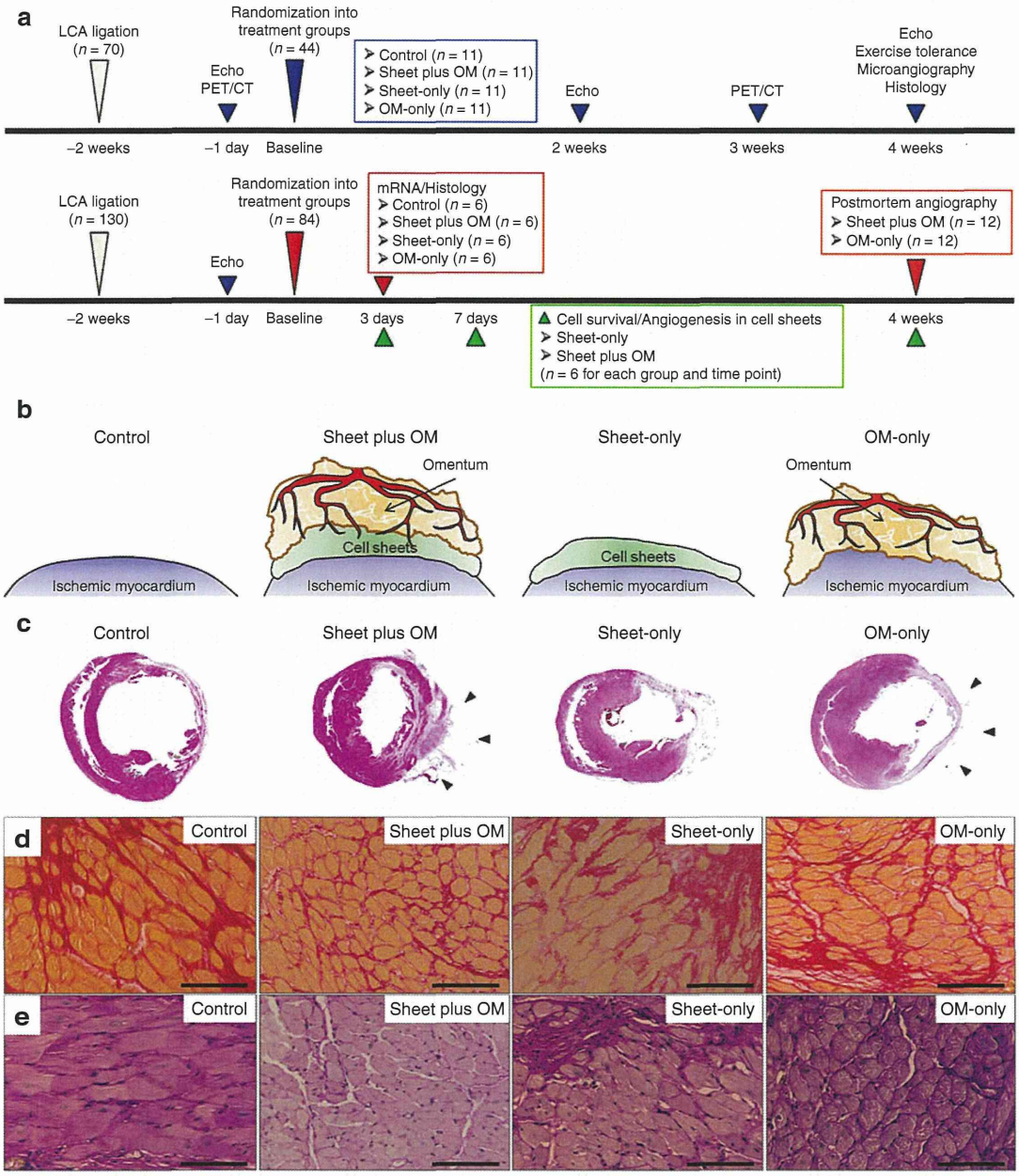

Figure 1 (**a**) Experimental protocols. (**b**) Procedural schemes for treatment groups. (**c**) Macroscopic images of HE-stained whole sections of the left ventricle and (**d**) anterior wall thickness (40×, scale bar = 1,000 μm). Black arrows indicate the omentum tissue. Photomicrographs of Sirius red- (**e**) and periodic acid-Schiff-stained (**f**) sections of peri-infarct myocardium (400×, scale bar = 100 μm) (n = 11 for each group).

The number of endothelial (CD31 positive) cells in the control and single treatment groups decreased with time, while that in the combined remained unchanged. Consequently, the angiogenic effects induced in the latter were more profound at 28 days after treatment, with a significantly greater amount of mature vessels (**Figure 4h–n**).

Number of resistance vessels and relative dilatory responses to endothelium-dependent stimulation in ischemic myocardium

To evaluate the effects of each treatment on microcirculation physiology in terms of relative dilatory responses to acetylcholine and dobutamine hydrochloride in the resistance vessels, synchrotron radiation microangiography was performed after 3 weeks after the treatment (control: n = 11, combined: n = 11, cell-sheet: n = 5, OM: n = 6). Using iodinated agents, coronary microcirculation in ischemic areas was clearly visualized in anesthetized closed-chest rats (**Figure 5a**). Vessel internal diameter (ID) at baseline (before agent administration) tended to decrease according to branching order and differed among the groups with larger first branching order arteries observed in the combined group (**Figure 5b**). Moreover, the combined group had a greater number of third and fourth branching order arterial vessels (resistance arterial vessels) at baseline (**Figure 5c**).

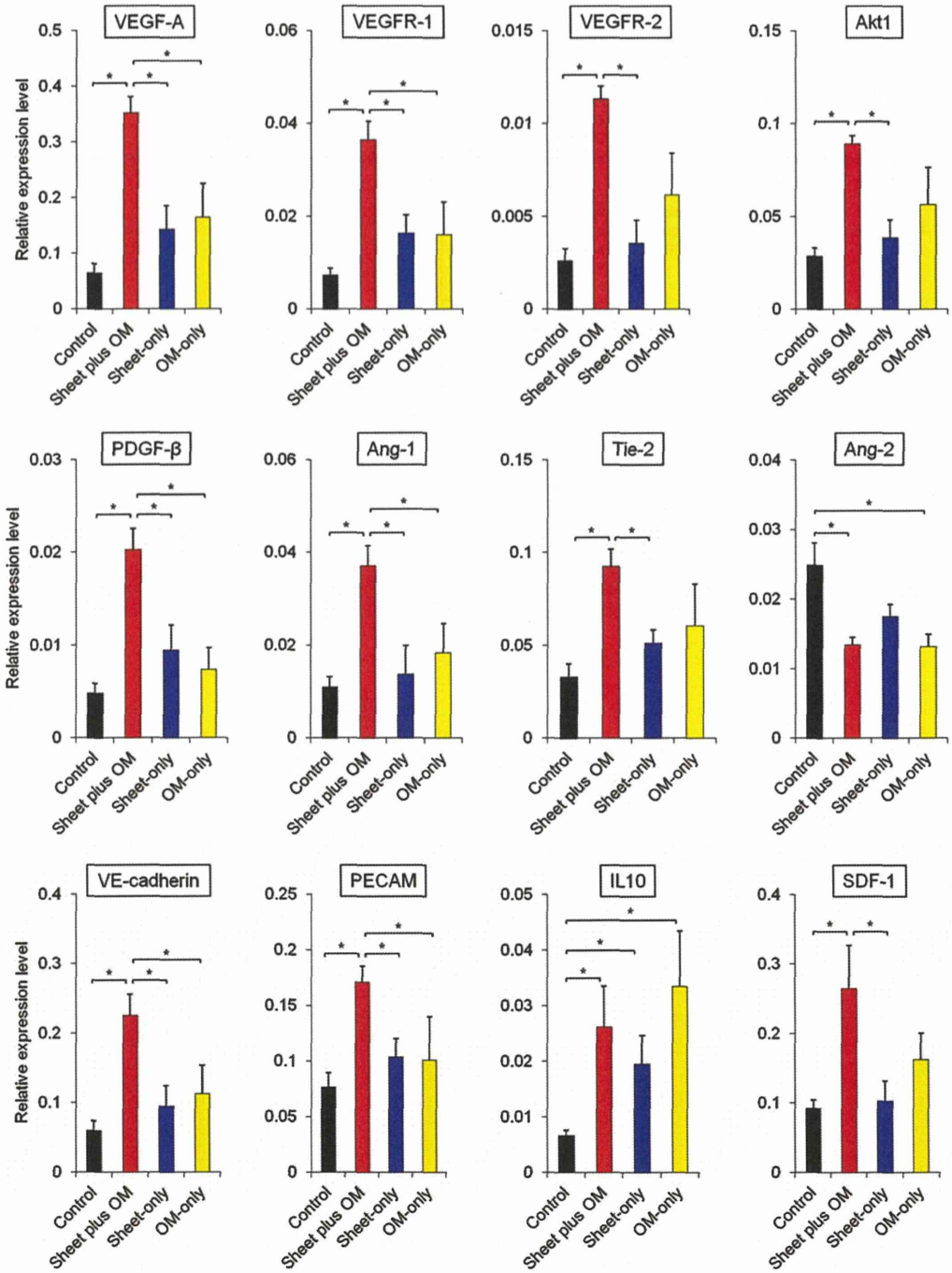

Figure 2 Quantitative reverse transcription PCR showing gene expressions related to angiogenesis, vessel maturation, and anti-inflammation in peri-infarct myocardium 3 days after treatment ($n = 6$ for each group) (*$P < 0.05$). Data were normalized to β-actin expression level. As compared to the others, the combined group showed substantially higher gene expressions associated with angiogenesis, vessel remodeling and anti-inflammation in peri-infarct myocardium at 3 days after treatment.

Acetylcholine-mediated dilation in the third and fourth branching orders was significantly different among the groups. The mean caliber changes in response to acetylcholine in the combined group were 28±8% and 32±8% for the third and fourth order branches respectively, which were greater than in the others (**Figure 5d**). Similarly, the mean caliber changes in response to dobutamine hydrochloride in the combined group were 31±7% and 34±7%, respectively, which were greater than in the others (**Figure 5e**).

The distributions of individual segment caliber changes in response to acetylcholine are described in **Supplementary Figure S1**. The control group had a relatively high frequency of third and fourth branching order arterial vessels showing localized segmental vasoconstriction (ID constriction >5% of baseline). The frequency of abnormal vasoconstriction with acetylcholine in the control group was about eight- and fourfold for the third and fourth branching order, respectively, as compared

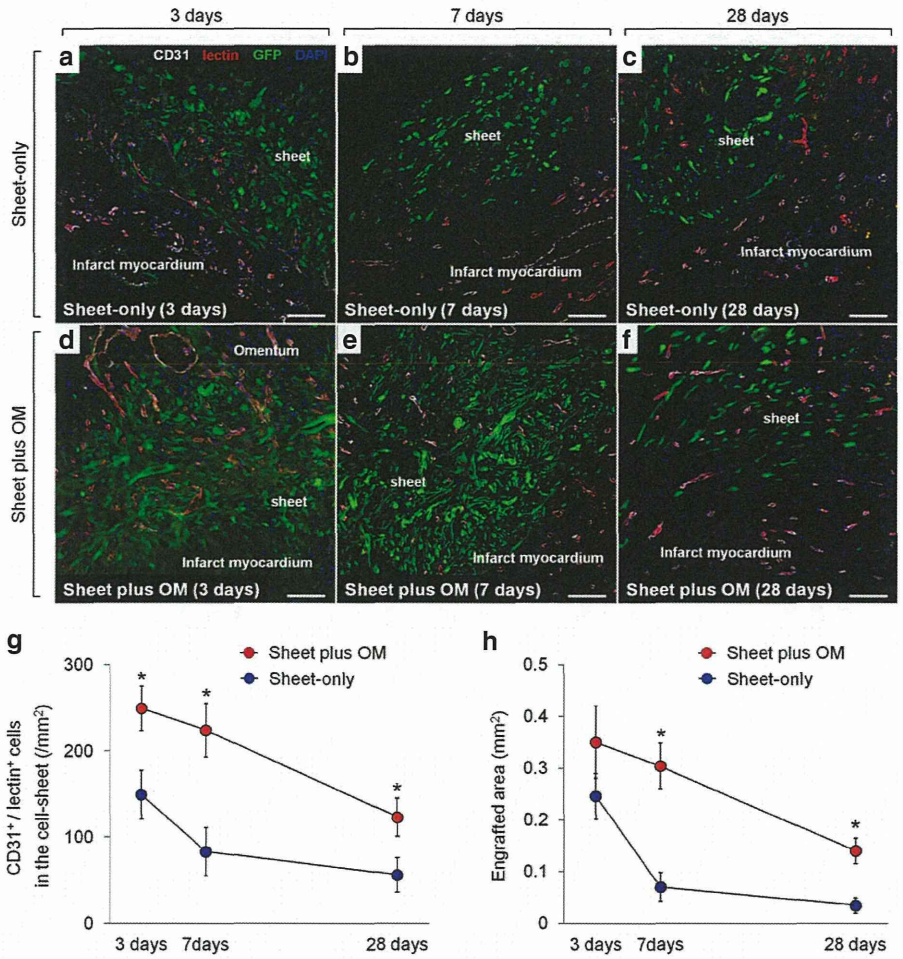

Figure 3 Serial representative images of functional blood vessels with patent endothelial layers (CD31/lectin double-positive) vessels in the transplanted donor (GFP-positive) cells in sheet-only (**a–c**) and combined groups (**d–f**) at 3, 7, and 28 days after each treatment (200×, scale bar = 100 μm). Quantitative analyses of functionally mature vessels in the transplanted area (**g**) and the donor (GFP-positive) cell presence (**h**) at 3, 7, and 28 days after each treatment ($n = 6$ for each group and each time point) (* $P < 0.05$ versus sheet-only group). At 3 days after treatment, in the sheet-only group, several blood vessels were just located at the border between the sheet and infarct area (**a**), whereas a large number of functional vessels was detected proximal to the border between the cell-sheet and OM and within the sheet in the combined group (**d**). Consequently, the combined group had greater numbers of functional blood vessels in the cell-sheet than the sheet-only group at any follow-up point (**g**). There was no significant difference in the engrafted area at 3 days after transplantation between the groups, while the subsequent changes in each group were apparently distinctive (**h**). During the 7 days after the treatment, the amount of decrease in the engrafted area was substantially smaller in the combined group than that in the sheet-only group, resulting in 4.3-fold increased retention of donor cells in the former group. This led to the greater donor cell presence in the combined group persistently (at least until day 28), which was consistent with the amount of vessel recruitment in the cell-sheet.

with the combined group (third order: control 49% versus combined 6% versus sheet-only 22% versus OM-only 25%; fourth order: control 18% versus combined 4% versus sheet-only 13% versus OM-only 17%).

Global and regional changes in myocardial blood flow and coronary flow reserve

To evaluate global and regional myocardial blood flow (MBF), and coronary flow reserve (CFR), ^{13}N-ammonia PET measurements were serially performed 1 day before and 3 weeks after the treatments (control: $n = 5$, combined: $n = 8$, cell-sheet: $n = 7$, OM: $n = 7$) (**Figure 6a–f**). In normal rats used for the validation study, global MBF at rest and during stress was 5.1 ± 0.5 and 7.1 ± 1.3 ml/min/g respectively, while global CFR was 1.4 ± 0.3.

Two weeks after coronary ligation (before treatment), global MBF at rest and during stress were substantially decreased in all groups, with no significant differences. Similarly, global CFR was not different among the groups. Three weeks after treatment, global MBF at rest was not different, while that during stress was significantly greater in the combined and single treatment groups as compared to the control (control 2.5 ± 0.4 versus combined 3.8 ± 0.6 versus sheet-only 3.3 ± 0.5 versus OM-only 3.8 ± 0.3, respectively, ANOVA p=0.0003). Postoperative global CFR was also substantially higher in the treatment groups as compared with the control (control 1.1 ± 0.2 versus combined 1.4 ± 0.2 versus sheet-only 1.4 ± 0.2 versus OM-only 1.4 ± 0.2, respectively, ANOVA p=0.015).

With regard to the magnitude of change in the global CFR (pre- versus post-treatment), the combined group offered the

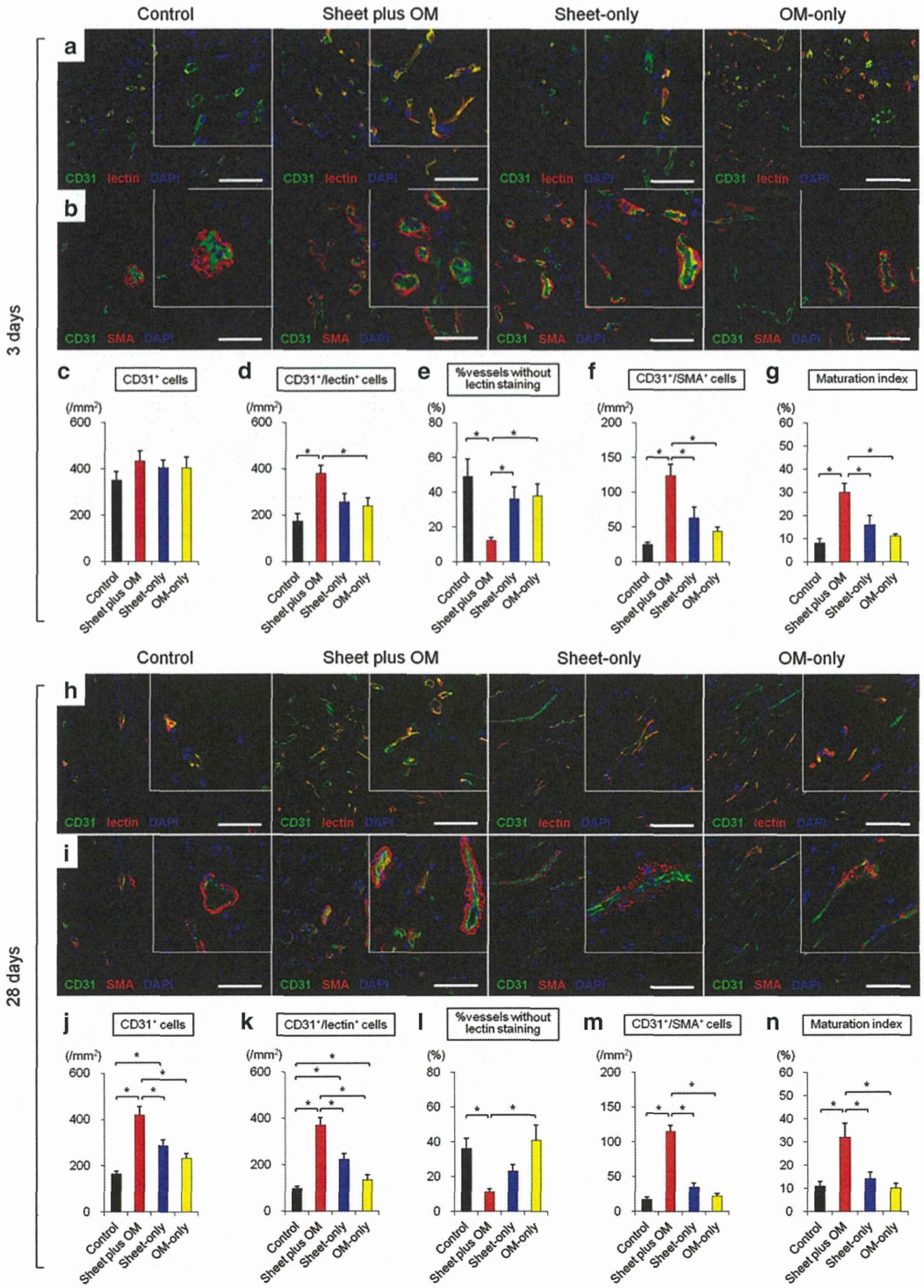

Figure 4 Immunohistochemical analyses of functionality (patency) and vessel maturation observed in peri-infarct myocardium at 3 ($n = 6$ for each group) (**a–g**) and 28 ($n = 11$ for each group) (**h–n**) days after treatments (* $P < 0.05$). Representative CD31/lectin and CD31/α-SMA staining at 3 (**a,b**) and 28 (**h,i**) days after treatments (400×, scale bar= 100 μm). Three days after treatment, there was no difference in number of CD31-positive cells among the groups, though the combined group showed a trend of greater number of functional blood vessels with patent endothelial layers (CD31/lectin double-positive) and structurally (CD31/α-SMA double-positive) mature vessels, with a higher maturation index (**c–g**). Notably, the percentage without lectin staining ($CD31^+/lectin^-$) was significantly smaller in the combined group. The number of endothelial (CD31 positive) cells in the control and single treatment groups decreased with time, while that in the combined remained unchanged. Consequently, the angiogenic effects induced in the latter were more profound at 28 days after treatment, with a significantly greater amount of mature vessels (**j–n**).

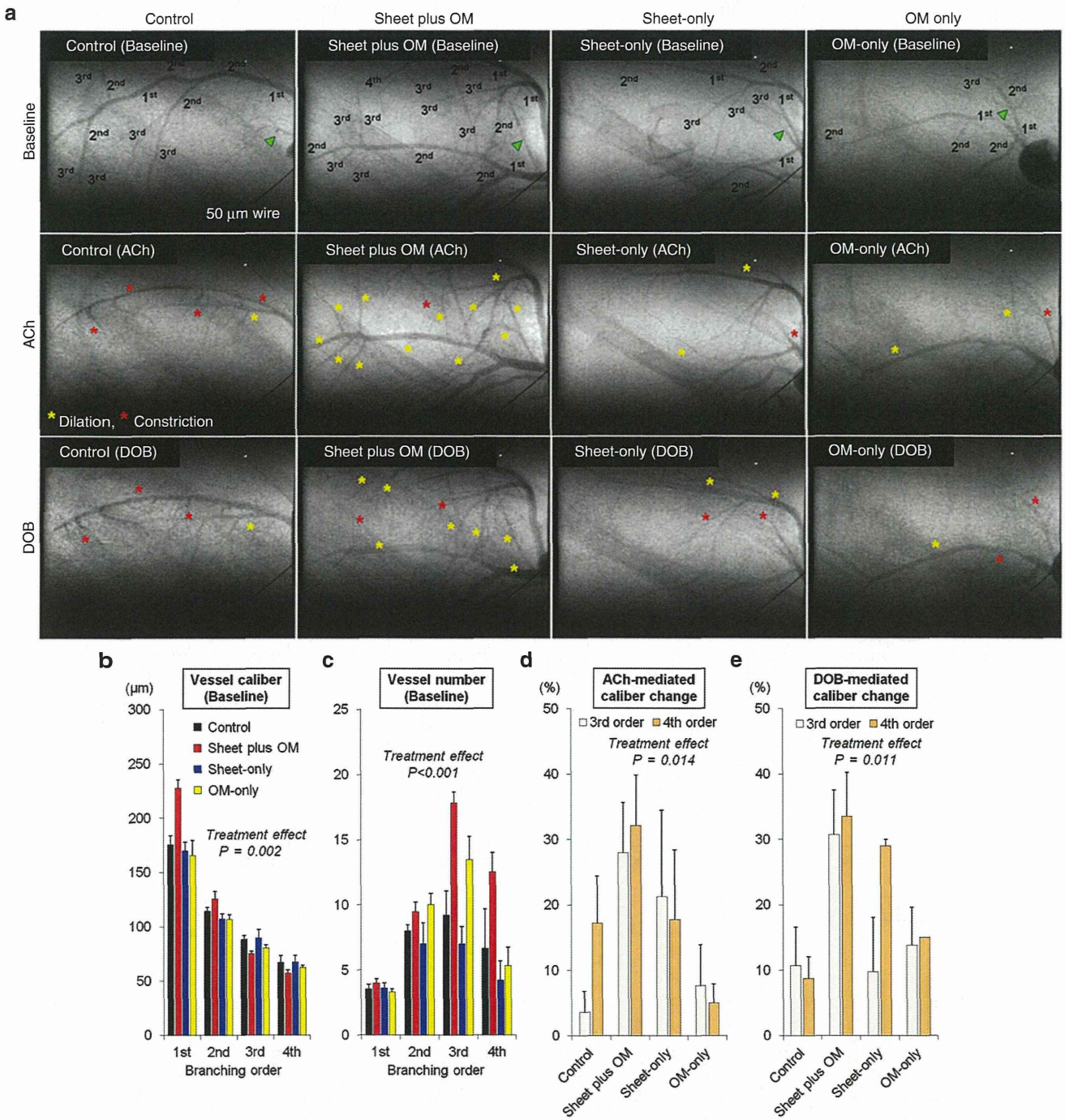

Figure 5 Synchrotron radiation microangiography was performed to evaluate vessel number and caliber and relative dilatory responses to acetylcholine and dobutamine hydrochloride in resistance vessels (control: $n = 11$, combined: $n = 11$, cell-sheet: $n = 5$, OM: $n = 6$). Using iodinated agents, coronary microcirculation in ischemic areas was clearly visualized in anesthetized closed-chest rats. Representative angiogram frames for all treatment groups at baseline, and in response to acetylcholine and dobutamine hydrochloride (**a**). Yellow and red asterisks indicate vessels showing dilation and constriction in response to acetylcholine and dobutamine hydrochloride, respectively. Quantitative analyses of (**b**) vessel internal diameter and (**c**) visible vessel number at baseline according to branching order. Vessel internal diameter at baseline (before agent administration) tended to decrease according to branching order and differed among the groups with larger first branching order arteries observed in the combined group (**b**). Moreover, the combined group had a greater number of third and fourth branching order arterial vessels (resistance arterial vessels) at baseline (**c**). Mean caliber changes in response to (**d**) acetylcholine and (**e**) dobutamine hydrochloride. Acetylcholine-mediated dilation in the third and fourth branching orders was significantly different among the groups. The mean caliber changes in response to acetylcholine in the combined group were 28±8% and 32±8% for the third and fourth order branches respectively, which were greater than in the others (**d**). Similarly, the mean caliber changes in response to dobutamine hydrochloride in the combined group were 31±7% and 34±7%, respectively, which were greater than in the others (**e**).

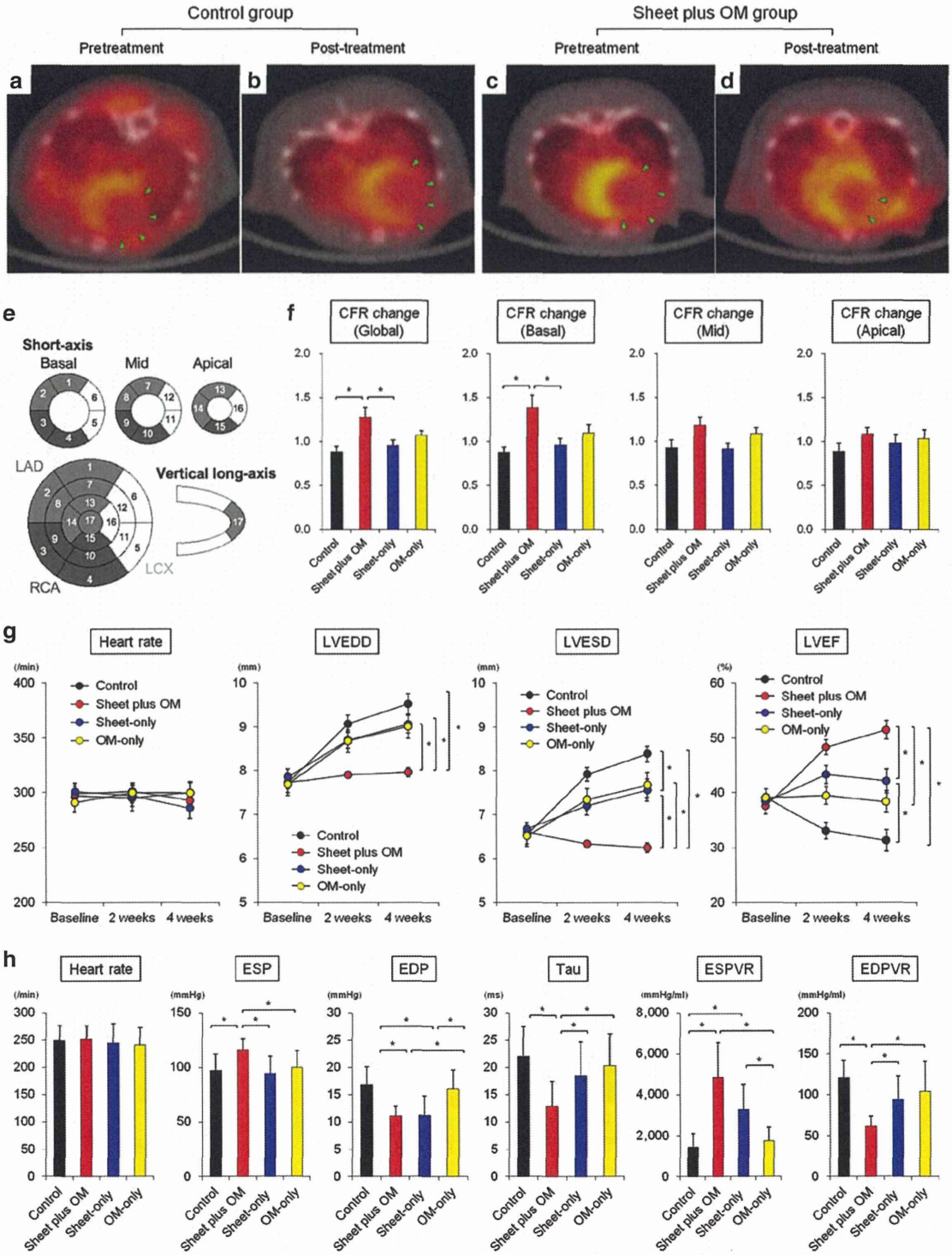

Figure 6 Representative serial PET/CT fusion images of ^{13}N-NH_3 PET during stress in control (**a**,**b**) and combined (**c**,**d**) groups. Recovery of MBF in large portion of basal left ventricle (anterior and lateral segments) was observed in the combined but not control group (green triangles). Quantitative analyses of changes in CFR calculated as a ratio of post-treatment to pretreatment CFR in global, basal, mid, and apical LV segments (control: $n = 5$, combined: $n = 8$, cell-sheet: $n = 7$, OM: $n = 7$) (*$P < 0.05$) (**e**,**f**). The combined group offered the most remarkable improvement in the global CFR, as evidenced by a higher ratio of post- to pretreatment CFR. Notably, that beneficial change was mainly caused by significant improvement in the basal left ventricle. CFR, coronary flow reserve; MBF, myocardial blood flow. (**g**) Serial assessments of cardiac function parameters at baseline (before treatment), and 2 and 4 weeks after treatments (*$P < 0.05$). In the combined group, remarkable improvements in LV function parameters occurred promptly and were sustained for up to 4 weeks, resulting in significantly smaller LV dimensions and greater LV ejection fraction as compared with other treatment groups. (**h**) Quantitative analyses of hemodynamic function parameters for each treatment (*$P < 0.05$). The basic hemodynamic indices revealed that LV end-systolic pressure was higher, whereas LV end-diastolic pressure and time constant were lower in the combined group as compared to the others. Pressure–volume loop analysis revealed that end-systolic pressure–volume relationship was higher, while end-diastolic pressure–volume relationship was lower in the combined group.

most remarkable improvement in the global CFR, as evidenced by a higher ratio of post- to pre-treatment CFR. Notably, that beneficial change was mainly caused by significant improvement in the basal left ventricle (control 0.9 ± 0.1 versus combined 1.4 ± 0.4 versus sheet-only 1.0 ± 0.1 versus OM-only 1.1 ± 0.1, respectively, ANOVA $P = 0.012$) (**Figure 6e,f**).

Global LV function and hemodynamic performance

The cardiac function was evaluated by echocardiography before (at baseline) and 2 and 4 weeks after each treatment ($n = 11$ for each group) (**Figure 6** g,h). Two weeks after left coronary artery ligation, severe dilatation of the LV chamber and severe systolic dysfunction were observed, with no significant differences among the groups (**Figure 6g**). In the control, LV dimensions increased and LV ejection fraction deteriorated in a time-dependent manner, suggesting progressive LV remodeling. In the sheet-only and OM-only groups, LV ejection fraction initially improved, then tended to deteriorate in association with gradual LV dilatation. In the combined group, remarkable improvements in LV function parameters occurred promptly and were sustained for up to 4 weeks, resulting in significantly smaller LV dimensions and greater LV ejection fraction as compared with other treatment groups.

Consistently, the basic hemodynamic indices revealed that LV end-systolic pressure was higher, whereas LV end-diastolic pressure and time constant were lower in the combined group as compared to the others. Load-independent parameters assessed by pressure–volume loop analysis revealed that end-systolic pressure–volume relationship was higher, while end-diastolic pressure–volume relationship was lower in the combined group (**Figure 6h**). These results confirmed that cell-sheet therapy combined with OM-flap improved the therapeutic effects of single treatment group (cell-sheet only or OM-flap only) for the treatment of chronic MI.

Functional capacity assessment

There was no difference in running distance at 4 rpm (control 125 ± 15 versus combined 148 ± 9 versus sheet-only 133 ± 10 versus OM-only 135 ± 15 m, ANOVA $P = 0.63$) ($n = 11$ in each). In contrast, the combined group showed more improved functional capacity in terms of longer running distance at 8 rpm (54 ± 5 versus 178 ± 17 versus 81 ± 10 versus 76 ± 7 m, respectively, ANOVA $P < 0.001$).

Angiographic assessment of communication between coronary arteries and pedicle omentum

Communication between the coronary arteries and branches of the gastroepiploic artery in the OM specimens was evaluated using three different methods with a different series of OM-only and combined group animals ($n = 12$ in each) (**Figure 1a**).

A postmortem angiography examination from the aortic root was performed to verify antegrade flow from the OM into the heart in the combined and OM-only groups ($n = 4$ for each group). In the combined group, aortography revealed that the gastroepiploic artery branches feeding the OM expanded into the heart, and established several tight junctions between the native coronary arteries and OM (**Figure 7a**). In contrast, in the OM-only group, the gastroepiploic artery branches failed to penetrate the heart, accompanied by immature leaky collateral vessel formation between the coronary artery and OM, evidenced by considerable leakage of contrast agent (**Figure 7b**).

We selectively injected India ink into the celiac artery to visually and histologically confirm vessel communication between the pedicle OM and native coronary artery ($n = 4$ for each group). Numerous collaterals filled with India ink were clearly identified between the gastroepiploic artery and native coronary arteries in the combined group, while that was not seen in the OM-only group (data not shown) (**Figure 7c–e**). Histological analysis confirmed vessel communication between those in the combined group (**Figure 7f,g**).

Finally, a selective perfusion via aortic root and celiac artery using two different MICROFIL colors was performed ($n = 4$ for each group). In the combined group, MICROFIL solution injected in a retrograde manner into the aortic root (MV-117 Orange) was easily shown expanded into the OM to communicate with the gastroepiploic artery (**Figure 7h**). That solution injected into the celiac artery (MV-120 Blue) was also found to expand into the myocardium and communicated with native coronary arteries (**Figure 7i**). Those findings were not seen in the OM-only group (data not shown).

Vessel migration into cell-sheet from host myocardium and omentum

To further confirm whether the OM- and host myocardium-derived endothelial cells migrated toward the cell-sheet, we established two types of parabiotic pair models ($n = 4$ for each).

In parabiotic pairs of wild-type MI rats that received transplantation of cell-sheets labeled with Cell Tracker TM Orange CMTMR followed by coverage with a GFP-transgenic rat oriented pedicle OM, a large number of OM-derived endothelial cells (isolectin/GFP double-positive cells) had migrated toward the cell-sheet (**Figure 8a–d**). Similarly, in another parabiotic pair of GFP-transgenic MI rats that received cell-sheet transplantation covered with a wild-type rat oriented pedicle OM, a large number of host myocardium-derived endothelial cells (isolectin/GFP double-positive cells) had migrated toward the cell-sheet (**Figure 8e–h**).

Cell-sheet stimulated vascular cell migration

We performed an *in vitro* migration assay using HUVECs to evaluate the effects of skeletal myoblast cell-sheet derived growth factors on vessel recruitment (**Figure 8i**). The number of migrating cells was significantly greater in the 100% conditioned medium group, followed by the 10% conditioned medium and control groups, suggesting that SM cell-sheet derived growth factors stimulate vascular cell migration in a concentration-dependent manner (**Figure 8j,k**).

DISCUSSION

The major findings of this study can be summarized as follows. As compared to the single treatment groups, the cell-sheet plus OM group showed (i) improved donor cell retention along with amplified angiogenesis in the cell-sheet through the follow-up (at least day 28), (ii) attenuated cardiac hypertrophy and

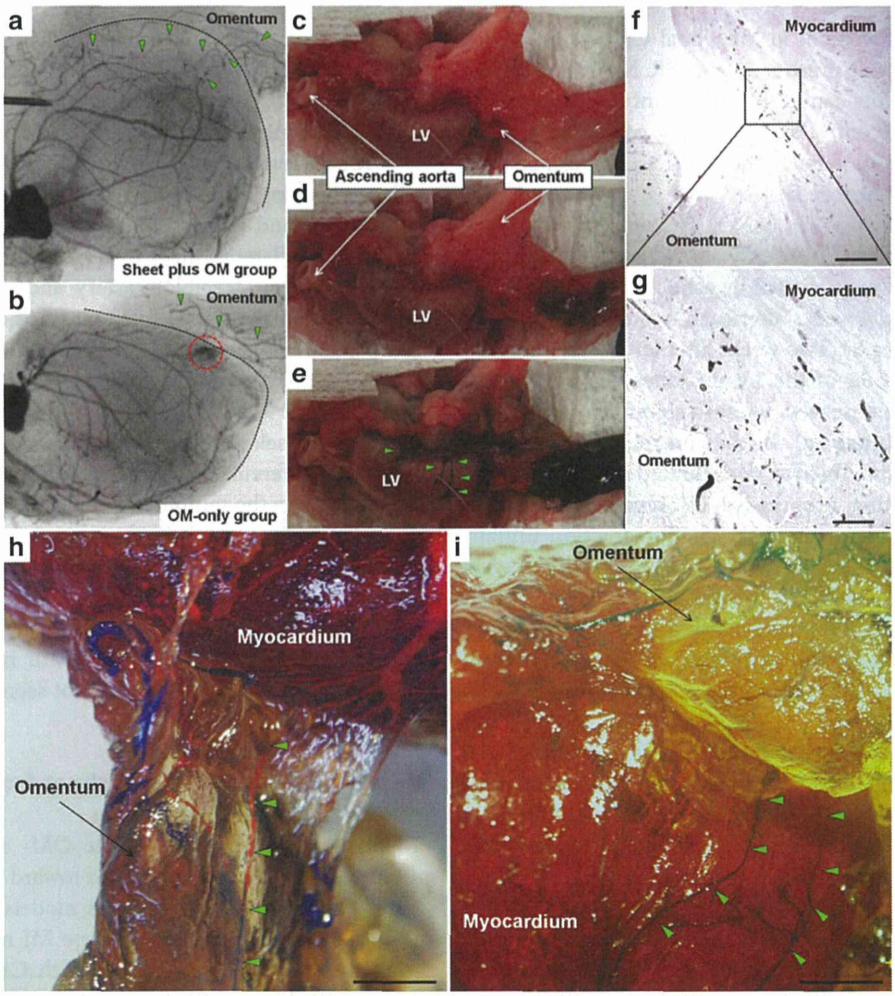

Figure 7 Communication between the coronary arteries and branches of the gastroepiploic artery was evaluated using three different methods with a different series of OM-only and combined group animals. A postmortem angiography examination from the aortic root in the combined (**a**) and OM-only (**b**) groups ($n = 4$ for each group). In the combined group, aortography revealed that the gastroepiploic artery branches feeding the OM expanded into the heart, and established several tight junctions between the native coronary arteries and OM (**a**). In contrast, in the OM-only group, the gastroepiploic artery branches failed to penetrate the heart, accompanied by immature leaky collateral vessel formation between the coronary artery and OM, evidenced by considerable leakage of contrast agent (red dotted circle) (**b**). Black dotted line indicates heart surface. Green triangles indicate the branches of the gastroepiploic artery. Selective India ink injection into the celiac artery to visually and histologically confirm vessel communication between the pedicle OM and native coronary artery ($n = 4$ for each group). Numerous collaterals filled with India ink were clearly identified between the gastroepiploic artery and native coronary arteries in the combined group (**c–e**), while that was not seen in the OM-only group (data not shown). Histological analysis confirmed vessel communication between those in the combined group (**f**: 40×, scale bar = 500 μm, **g**: 200×, scale bar = 100 μm). A selective perfusion via aortic root and celiac artery using two different MICROFIL colors ($n = 4$ for each group). In the combined group, MICROFIL solution injected in a retrograde manner into the aortic root (MV-117 Orange) was easily shown expanded into the OM to communicate with the gastroepiploic artery (**h**, 7.5×, scale bar = 2 mm). That solution injected into the celiac artery (MV-120 Blue) was also found to expand into the myocardium and communicated with native coronary arteries (**i**, 7.5×, scale bar = 2 mm). Those findings were not seen in the OM-only group (data not shown). Green triangles show visible vessel communication in the OM-flap (**h**) and host myocardium (**i**).

fibrosis, and a greater amount of functionally and structurally mature blood vessels in the ischemic myocardium, along with myocardial upregulation of relevant genes, (iii) increased vascularization in resistance arterial vessels with better dilatory responses to endothelium-dependent agents, (iv) more remarkable improvement in the global CFR, mainly caused by significant improvement in the basal left ventricle, (v) sustained improvements in cardiac function parameters and better functional capacity, and (vi) creation of robust vascular communication between the OM and native coronary arteries, shown by *in vivo* angiography.

The retention, survival, and engraftment of transplanted cells in the cell-sheet therapy are largely influenced by the degree of vascularization in the transplanted area and subsequent myocardial inflammation after cell-sheet transplantation.[2,17] The concept of combining OM-flap with the current cell-sheet therapy is likely to be reasonable because the OM is known to play a key role in controlling the spread of inflammation, and promoting revascularization, reconstruction and tissue regeneration. Our data suggest that the combined treatment improved the hypoxic environment in the transplanted area to a greater degree, potentially enhancing initial cell engraftment and enhancing the paracrine

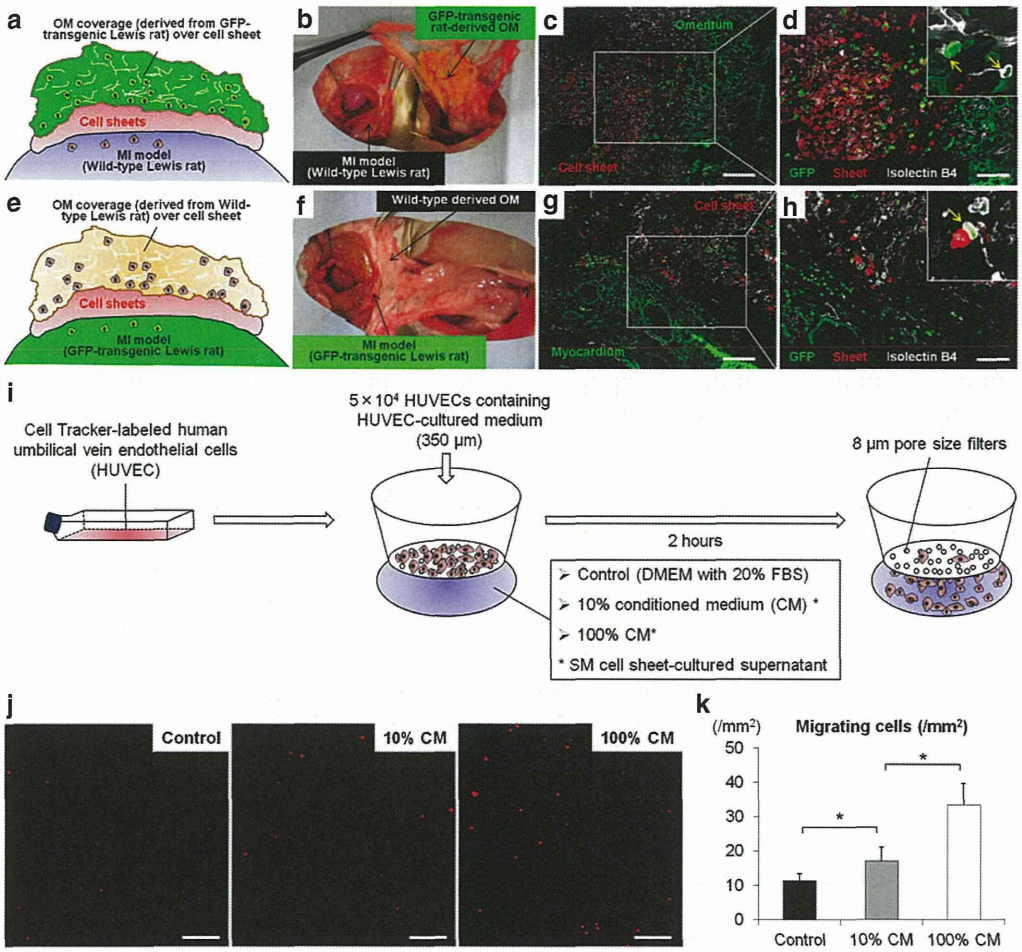

Figure 8 Schematic representation of experimental design to form parabiotic pairs of wild-type MI model rats (recipient) for transplantation of wild-type oriented cell-sheets labeled with Cell Tracker TM Orange CMTMR, followed by coverage with pedicle OM derived from GFP-transgenic rat (donor) (**a**,**b**). Representative GFP/isolectin staining in parabiotic pairs model (**c**: 100×, scale bar = 200 μm, **d**: 200×, scale bar = 100 μm). Schematic representation of experimental design to form second parabiotic pairs of GFP-transgenic MI rats for cell-sheet transplantation covered with wild-type oriented pedicle OM (**e**,**f**). Representative GFP/isolectin staining in second parabiotic pairs (**g**: 100×, scale bar = 200 μm, **h**: 200×, scale bar = 100 μm). *In vitro* migration assay (**i**). To investigate cell migration in response to skeletal myoblast cells cultured in conditioned medium, a modified Boyden chamber migration assay was performed using an HTS FluoroBlok Multiwell Insert System containing filters with a pore size of 8 μm. Human umbilical vein endothelial cells (HUVECs) were grown in EGM-2 culture medium. After incubation at 37 °C for 2 hours, the number of migrated cells was counted in 15 randomly chosen fields under 100× magnification using fluorescence microscopy. Two replicate samples were used in each experiment, which were performed at least twice. Migrating cells were analyzed using a light microscope and reported as numbers of migrating cells per mm² (**j**). Representative images show migrating cells labeled with Cell Tracker TM Orange CMTMR (100×, scale bar = 200 μm). Quantitative analyses of migrating cells according to concentration in the skeletal myoblast-cultured conditioned medium (**k**). Asterisk indicates statistical significance ($P < 0.05$).

effects induced by cell-sheet therapy in terms of higher expressions of relevant genes, potentially stabilizing therapeutic effect of cell-sheet therapy. The discrepancy between functional improvement and donor cell engraftment suggests that the improvement of cardiac function is not mainly mediated by direct contribution of transplanted donor cells but other indirect roles, possibly paracrine effects, offered by the cell-sheet at the early stage of transplantation.

The histological findings demonstrated that the rats receiving the cell-sheet implantation plus OM-flap had a significantly thickened anterior LV wall that was augmented by cardiomyocyte layers as compare to the other groups. Potential mechanisms may include cardiomyogenic differentiation of the donor-derived cells or endogenous stem cells, or paracrinal inhibition of progressive necrosis and/or apoptosis of the native cardiomyocytes. We speculate that both mechanisms might have contributed to the thickening of the targeted LV wall, although cardiomyogenic differentiation was not clearly identified in this study. Improved regional blood flow by the combined therapy could reduce the number of the necrotic/apoptotic cardiomyocytes, while reduced accumulation of fibrous components would inhibit thinning of the LV wall.[5,18] In addition, girdling effects from the covered OM might have reduced wall stress of the LV, leading to maintenance of the LV thickness.[19] Further studies to focus on the cardiomyogenic transdifferentiation using genetically labeled rodent models are warranted.

When blood vessels grow, endothelial cells migrate out first and assemble in a primitive network of immature channels